Implicit Integrations

in Elasto–Plastic Geotechnics

Boris Jeremić [‡]   Stein Sture [§]

[‡]Graduate research assistant,

Department of Civil, Environmental, and Architectural Engineering,

Campus Box 428,

University of Colorado, Boulder, Colorado 80309-0428, U.S.A.

Email: Boris.Jeremic@Civil.Colorado.edu

[§]Professor and Chairman,

Department of Civil, Environmental, and Architectural Engineering,

Campus Box 428,

University of Colorado, Boulder, Colorado 80309-0428, U.S.A.

Email: Stein.Sture@Civil.Colorado.edu

Abstract

The paper presents derivation of a fully implicit Newton algorithm for direct integration of constitutive equations, in extended stress – internal variable space, involving hardening or softening of a general dilatant isotropic elasto–plastic geo-material. All relevant derivatives are provided in tensor notation, thus facilitating implementation. The consistent, algorithmic tangent stiffness tensor is derived. The relative accuracy of a template algorithm is assessed on a number of examples by means of iso–error maps. We present a rather simple, one–increment example concerning convergence properties of the Newton iterative scheme at the global, finite element level, associated with the consistent tangent stiffness tensor for integrating the weak form of the equilibrium equations.

Key Words: Elastoplasticity, Pressure sensitive materials, Constitutive modeling, Dilatancy, Inplicit Integrations.

1   Introduction

In recent years the focus in numerical elasto–plasticity has been on developing accurate and robust constitutive drivers. A number of schemes has been developed and their accuracy and stability have been tested. Fully implicit schemes, such as the Backward Euler scheme, that are able to integrate the constitutive equations for rather large, finite strain increments, have been developed for *simple materials*. Many complex models relevant for geomaterials have not benefited from this scheme, since they require formation of higher derivatives of the potential function in general stress space, and inclusion of hardening or softening behavior in the implicit scheme.

In this paper we derive the fully implicit Newton algorithm for a general hardening or softening, three – stress invariant isotropic material. It should be mentioned that Crisfield[?] has developed a simple Newton implicit algorithm, but it is only valid for perfect plasticity von Mises model. In this work we provide detailed derivation of all relevant derivatives in tensor notation. A comprehensive set of programming tools, here named the **nDarray**, was developed and used to facilitate the implementation of the derived tensor formulae in a versatile constitutive driver. The underlying motivation for this work is to develop a robust, and efficient *template constitutive driver*, which provides a solid base for a

simple implementation of different isotropic elasto–plastic material models. The driver is tested on a rather comprehensive, pressure sensitive, three – stress invariant, hardening or softening MRS–Lade elasto–plastic material model.[?]

The outline of this presentation is as follows. First we present a brief summary of elasto–plastic incremental theory. Our focus is on the specific subset of midpoint algorithms, the fully implicit, Backward Euler algorithm. We develop a fully implicit algorithm for direct integration of elasto–plastic constitutive equations in extended *stress – internal variable* space. Next, the derivation of the consistent tangent stiffness tensor is presented. A brief review of the MRS–Lade material model and a new accuracy measure are also presented. Then we describe an exercise involving a one step increment along the iterative stress path. The accuracy of the algorithm applied to the MRS–Lade model is then assessed using iso–error maps on a number of stress regions. A brief overview of convergence properties involving a consistent stiffness tensor is given by following one increment and the contained iterations for finite element analysis of a loose sand. Finally, in the Appendix, we present several useful formulae, namely the derivatives of general isotropic yield and potential functions in closed form as well as in a finite difference form.

2 Elasto–plasticity

2.1 Preliminaries

In selecting the appropriate integration scheme, a number of issues must be addressed. A special concern in computational mechanics applied to soils, is the possibility of significant changes in magnitude and direction of stresses and strains. A reliable constitutive driver should account for: *(a)* proper formulation of plastic loading – elastic unloading criteria, *(b)* existence of the integrated solution, *(c)* satisfaction of one or more yield criteria simultaneously, *(d)* stability and accuracy and *(e)* robustness and efficiency. The approach implemented most frequently in the early years was explicit, often resulting in unstable and inaccurate solutions, yet, a large number of principles developed at that time are still used.

2.2 Constitutive Relations for Infinitesimal Plasticity

The constitutive equations which characterize an elasto–plastic material can briefly be stated as follows: equations:

$$d\epsilon_{ij} = d\epsilon_{ij}^e + d\epsilon_{ij}^p \tag{1}$$

$$d\sigma_{ij} = E_{ijkl} d\epsilon_{kl}^e \tag{2}$$

$$d\epsilon_{ij}^p = d\lambda \, \frac{\partial Q}{\partial \sigma_{ij}} = d\lambda \, m_{ij}(\sigma_{ij}, q_*) \tag{3}$$

$$dq_* = d\lambda \, h_*(\sigma_{ij}, q_*) \tag{4}$$

where, $d\epsilon_{ij}$, $d\epsilon_{ij}^e$ and $d\epsilon_{ij}^p$ are increments of the total, elastic and plastic strain tensors respectively, $d\sigma_{ij}$ is the increment of Cauchy stress tensor, and dq_* represents increment for suitable set of internal variables. The asterisk in the place of indices in q_* replaces n indices[1]. Equation (1) expresses the assumed additive decomposition of the infinitesimal strain tensor into elastic and plastic parts. Equation (2) represents the generalized Hooke's law which linearly relates stresses and elastic strains increments through the modulus tensor E_{ijkl}. Equation (3) expresses a generally non-associated flow rule for the plastic strain, and equation (4) describes a set of hardening laws, that govern the evolution of the plastic variables. Tensor m_{ij} is the plastic flow direction, h_* the plastic moduli and $d\lambda$ is a plastic parameter to be determined with the aid of the loading—unloading criterion, which can be expressed in terms of the Karush–Kuhn–Tucker form as:

$$F(\sigma_{ij}, q_*) \leq 0 \tag{5}$$

$$d\lambda \geq 0 \tag{6}$$

$$F \, d\lambda = 0 \tag{7}$$

In the previous equations $F(\sigma_{ij}, q_*)$ denotes the yield function of the material and (5) characterizes the corresponding elastic domain. During any process of loading, conditions (5), (6) and (7) *must hold simultaneously*. For $F < 0$, equation (7) yields $d\lambda = 0$, i.e. elastic behavior, while plastic flow is characterized by $d\lambda > 0$, which with (7) is possible

---

[1]for example (q_{ij}) if the variable is ϵ_{ij}^p, or nothing (q) if the variable is a scalar value.

only if the yield criterion is satisfied, i.e. $F = 0$. From the latter constraint, and during the process of plastic loading the consistency condition is obtained in the form:

$$dF = \frac{\partial F}{\partial \sigma_{ij}} d\sigma_{ij} + \frac{\partial F}{\partial q_*} dq_* = n_{ij} d\sigma_{ij} + \xi_* dq_* = 0 \tag{8}$$

Equation (8) has the effect of confining the stress trajectory to the yield surface[2]. It is worthwhile noting that n_{ij} and ξ_* are normals to the yield surface in stress space and the plastic variable space respectively.

3 Backward Euler Integration Rule

In this section, we focus on the *Backward Euler algorithm*. The advantage of the Backward Euler scheme over other midpoint schemes is that the solution is sought by using the flow direction, $m_{ij} = \partial Q / \partial \sigma_{ij}$ at the final stress state. By *implicitly* assuming that such a stress state exists, the Backward Euler scheme is guaranteed to provide a solution, despite the size of the strain step. Furthermore, we present a complete derivation of a consistent tangent stiffness tensor for a pressure sensitive three–stress invariant isotropic material undergoing general hardening or softening.

3.1 Preliminaries

Fully implicit, Backward Euler schemes are given in the following form:

$$^{n+1}\sigma_{ij} = E_{ijkl} \left(^{n+1}\epsilon_{kl} - {}^{n+1}\epsilon_{kl}^{p} \right) \tag{9}$$

$$^{n+1}\epsilon_{ij}^{p} = {}^{n}\epsilon_{ij}^{p} + \lambda \, ^{n+1}m_{ij} \tag{10}$$

$$^{n+1}q_* = {}^{n}q_* + \lambda \, ^{n+1}h_* \tag{11}$$

$$F_{n+1} = 0 \tag{12}$$

where:

$$^{n+1}m_{ij} = m_{ij} \left(^{n+1}\sigma_{ij}, {}^{n+1}q_* \right) \tag{13}$$

[2]Since it only constitutes a linear expansion, the stress trajectory is confined to the tangential plane only.

$$^{n+1}h_* = h_* \left(^{n+1}\sigma_{ij}, ^{n+1}q_* \right) \tag{14}$$

Equations (9), (10), (11) and (12), are the nonlinear algebraic equations to be solved for the unknowns $^{n+1}\sigma_{ij}$, $^{n+1}\epsilon_{ij}^p$, $^{n+1}q_*$ and λ.

From Figure (1) it can be seen[3] that the Backward Euler rule may be regarded as a *return mapping algorithm*, where the elastic predictor stress $^{pred}\sigma_{ij}$ is projected on the updated yield surface along the flow direction evaluated at the final point $(^{n+1}\sigma_{ij}, ^{n+1}q_*)$.

3.2   Backward Euler Algorithm

The Backward Euler algorithm is based on the *elastic predictor – plastic corrector* strategy:

$$^{n+1}\sigma_{ij} = ^{pred}\sigma_{ij} - \lambda \, E_{ijkl} \, ^{n+1}m_{kl} \tag{15}$$

where $^{pred}\sigma_{ij} = E_{ijkl} \, \epsilon_{kl}$ is the elastic trial stress state and $^{n+1}m_{kl} = (\partial Q / \partial \sigma_{kl})|_{n+1}$ is the gradient to the plastic potential function in stress space at the final stress position.

If our predictor stress $^{pred}\sigma_{ij}$ is not located in a corner or apex gray region (for the material models that have these features), a single vector return to the yield surface is possible. It is advantageous to define a *tensor of residuals* r_{ij} as:

$$r_{ij} = \sigma_{ij} - \left(^{pred}\sigma_{ij} - \lambda \, E_{ijkl} \, ^{n+1}m_{kl} \right) \tag{16}$$

This tensor represents the difference between the current stress state σ_{ij} and the Backward Euler stress state $^{pred}\sigma_{ij} - \lambda \, E_{ijkl} \, ^{n+1}m_{kl}$. An initial estimate for the current stress $^{n+1}\sigma_{ij}$ can be obtained using various other methods, which will be discussed shortly. This estimate generally does not satisfy the yield condition, thus an iterative scheme is necessary to return the stress to the yield surface. The trial stress state $^{pred}\sigma_{ij}$ is maintained fixed during the iteration process. The first order Taylor series expansion can be applied to the equation (16) to obtain the iterative change, the *new* residual $^{new}r_{ij}$ from the old $^{old}r_{ij}$:

$$^{new}r_{ij} = ^{old}r_{ij} + d\sigma_{ij} + d\lambda E_{ijkl} \, ^{n+1}m_{kl} + \lambda E_{ijkl} \left. \frac{\partial m_{kl}}{\partial \sigma_{mn}} \right|_{n+1} d\sigma_{mn} + \lambda E_{ijkl} \left. \frac{\partial m_{kl}}{\partial q_*} \right|_{n+1} dq_* \tag{17}$$

---

[3]it should be pointed out that the vectors, as drawn on this figure, are pointing in the right direction only if we assume that $E_{ijkl} \equiv I_{ijkl}$. For any general elasticity tensor E_{ijkl} all vectors are defined in the E_{ijkl} metric, so the term "normal", as we are used to it, does not apply here.

where $d\sigma_{ij}$ is the change in σ_{ij}, $d\lambda$ is the change in λ, and $\partial m_{kl}/\partial \sigma_{mn} d\sigma_{mn} + \partial m_{kl}/\partial q_* dq_*$ is the change in m_{kl}. Upon setting ${}^{new}r_{ij} = 0$, and after some algebraic manipulations we are able to solve the previous equation for $d\sigma_{mn}$:

$$d\sigma_{mn} = -\left({}^{old}r_{ij} + d\lambda \, E_{ijkl} \, {}^{n+1}H_{kl}\right)\left({}^{n+1}T_{ijmn}\right)^{-1} \tag{18}$$

where we have introduced the fourth order tensors T_{ijmn} and H_{ijmn}:

$$ {}^{n+1}T_{ijmn} = \delta_{im}\delta_{nj} + \lambda \, E_{ijkl} \, \left.\frac{\partial m_{kl}}{\partial \sigma_{mn}}\right|_{n+1} \quad ; \quad {}^{n+1}H_{kl} = {}^{n+1}m_{kl} + \lambda\left.\frac{\partial m_{kl}}{\partial q_*}\right|_{n+1} h_* \tag{19}$$

A first order Taylor series expansion of the yield function F about the final stress state ${}^{n+1}\sigma_{ij}$ is applied in order to obtain a linear approximation of the new value of yield function ${}^{n+1}F^{new}$ with regard to changes in σ_{ij} and q_*:

$$ {}^{n+1}F^{new} = {}^{n+1}F^{old} + {}^{n+1}n_{mn} \, d\sigma_{mn} + {}^{n+1}\xi_* dq_* = 0 \tag{20}$$

where $n_{mn} = \partial F/\partial \sigma_{mn}$, $\xi_* = \partial F/\partial q_*$ and $dq_* = d\lambda \, h_*(\sigma_{ij}, q_*)$. We have the solution for $d\sigma_{mn}$ from equation (18), and by setting ${}^{n+1}F^{new} = 0$, the solution for $d\lambda$ is readily found:

$$ d\lambda = \frac{{}^{n+1}F^{old} - {}^{n+1}n_{mn} \, {}^{old}r_{ij} \, {}^{n+1}T^{-1}_{ijmn}}{{}^{n+1}n_{mn}E_{ijkl} \, {}^{n+1}H_{kl} {}^{n+1}T^{-1}_{ijmn} - {}^{n+1}\xi_* \, h_*} \tag{21}$$

Finally, with the solutions for $d\lambda$ from equation (21) and the solution for $d\sigma_{mn}$ from equation (18) we can write the iterative solution for $d\sigma_{mn}$ and dq_*, i.e. the solution in the *extended stress − internal variable space*, in the following form:

$$ d\sigma_{mn} = -\left({}^{old}r_{ij} + \frac{{}^{n+1}F^{old} - {}^{n+1}n_{mn} \, {}^{old}r_{ij} \, {}^{n+1}T^{-1}_{ijmn}}{{}^{n+1}n_{mn}E_{ijkl} \, {}^{n+1}H_{kl} {}^{n+1}T^{-1}_{ijmn} - {}^{n+1}\xi_* \, h_*} \, E_{ijkl} \, {}^{n+1}H_{kl}\right){}^{n+1}T^{-1}_{ijmn} \tag{22}$$

$$ dq_* = \left(\frac{{}^{n+1}F^{old} - {}^{n+1}n_{mn} \, {}^{old}r_{ij} \, {}^{n+1}T^{-1}_{ijmn}}{{}^{n+1}n_{mn}E_{ijkl} \, {}^{n+1}H_{kl} {}^{n+1}T^{-1}_{ijmn} - {}^{n+1}\xi_* \, h_*}\right) h_* \tag{23}$$

This iterative procedure is continued until the yield criterion $F = 0$ is satisfied given a certain tolerance, at the final stress state. It should be noted that in the case when our predictor point falls within the apex or corner gray area, we apply Koiter's rule. This is particularly the case if we use Mohr–Coulomb or the MRS–Lade material models.

3.3 Starting Points

It is well known that the rate of convergence, if there were to be convergence at all, for the *Newton Method,* is closely tied to the starting point of the iterative procedure. Less than favorable starting points might lead a Newton type algorithm to divergence or oscillatory behavior. In what follows, starting points for the Newton iterative procedure will be established for one–vector return algorithms. The case of two–vector returns, which appears for example in a cone–cap type yield surfaces, is treated in detail by Jeremić and Sture.[?]

3.3.1 Semi Backward Euler Starting Point

One of the proposed starting points,[(?)] uses the normal at the elastic trial point[4] $^{pred}\sigma_{ij}$. A first order Taylor expansion about point $^{pred}\sigma_{ij}$ yields:

$$^{pred}F^{new} = {}^{pred}F^{old} + {}^{pred}n_{mn}\, d\sigma_{mn} + \xi_* h_* d\lambda = 0 \tag{24}$$

It is assumed that the total incremental strain ϵ_{kl} is applied in order to reach the point $^{pred}\sigma_{ij}$, i.e. $^{pred}\sigma_{ij} = E_{ijkl}\, \epsilon_{kl}$ so that any further stress "relaxation" toward the yield surface takes place under a zero total strain condition, $\epsilon_{kl} = 0$. From the differential form of equation (9) and equation (24) the solution for $d\lambda$ is readily found:

$$d\lambda = \frac{^{pred}F^{old}}{^{pred}n_{mn}\, E_{mnpq}\, {}^{pred}m_{pq} - \xi_* h_*} \tag{25}$$

With this solution for $d\lambda$ we can obtain the starting point for the *Newton iterative procedure* as:

$$^{start}\sigma_{mn} = E_{mnpq}\, {}^{pred}\epsilon_{pq} - E_{mnpq}\, \frac{^{pred}F^{old}}{^{pred}n_{mn}\, E_{mnpq}\, {}^{pred}m_{pq} - \xi_* h_*}\, {}^{pred}m_{pq} \tag{26}$$

$$^{start}q_* = {}^{previous}q_* + \left(\frac{^{pred}F^{old}}{^{pred}n_{mn}\, E_{mnpq}\, {}^{pred}m_{pq} - \xi_* h_*} \right) {}^{pred}h_* \tag{27}$$

This starting point in extended stress – internal variable space will in general not satisfy the yield condition $F = 0$, but it will provide an initial estimate for the *Newton iterative procedure.*

---

[4]We have named this scheme as *semi Backward Euler scheme.*

It should be mentioned, that this scheme for returning to the yield surface is the well known *Radial Return Algorithm* , if the yield criterion under consideration is of the *von Mises* type. In this special case the normal at the elastic trial point $^{pred}\sigma_{ij}$ coincides with the normal at the final stress state $^{n+1}\sigma_{ij}$, and the return direction is exact. Similar scheme was used by de-Borst[?] and Crisfield[?] in conjunction with Mohr–Coulomb yield surface.

3.3.2 Forward Euler Starting Point

Another readily available and possible starting point can be obtained by applying one *Forward Euler step.* To be able to use the Forward Euler integration scheme, an intersection point has to be found.[?] Similarly to the previous derivation, a first order Taylor expansion about intersection point $^{cross}\sigma_{ij}$ yields:

$$F^{new} = \ ^{cross}n_{mn} \ d\sigma_{mn} + \xi_* h_* d\lambda = 0 \tag{28}$$

From the differential form of equation (9) and from the equation (28) $d\lambda$ is readily found:

$$d\lambda = \frac{^{cross}n_{mn} \ E_{mnpq} \ d\epsilon_{pq}}{^{cros}n_{mn} \ E_{mnpq} \ ^{cros}m_{pq} - \xi_* h_*} \tag{29}$$

With this solution for $d\lambda$ we can obtain the starting point for the *Newton iterative procedure*:

$$^{start}\sigma_{mn} = E_{mnpq} \ d\epsilon_{pq} - E_{mnpq} \ \frac{^{cross}n_{rs} \ E_{rstu} \ d\epsilon_{tu}}{^{cross}n_{ab} \ E_{abcd} \ ^{cross}m_{cd} - \xi_* h_*} \ ^{cross}m_{pq} \tag{30}$$

$$^{start}q_* = \ ^{previous}q_* + \left(\frac{^{cross}n_{mn} \ E_{mnpq} \ d\epsilon_{pq}}{^{cros}n_{mn} \ E_{mnpq} \ ^{cros}m_{pq} - \xi_* h_*} \right) h_* \tag{31}$$

This starting point will, again, not satisfy the yield condition $F = 0$ (except for yield criteria that have flat yield surfaces (in the stress invariant space) so that the first order Taylor linear expansion is exact), but will provide an initial estimate for the *Newton iterative procedure.* If the Newton iterative scheme fails to converge within prescribed number of steps, say 20, one has to provide continuation of the solution procedure by means of, for example a subincrementation technique, or by applying one of the line search techniques to the iterative algorithm.

3.4 Consistent Tangent Stiffness Tensor

The final goal in deriving the Backward Euler scheme for integration of elasto–plastic constitutive equations is to use that scheme in finite element computations. If the Newton iterative scheme is used at the global equilibrium level, then the use of the so called traditional, continuum tangent stiffness tensor destroys the quadratic rate of asymptotic convergence of the iterative scheme. In order to preserve such a quadratic rate, a *consistent, algorithmic,* tangent stiffness tensor should be derived. The consistent tangent stiffness tensor makes use of derivatives of direction ($m_{ij} = \partial Q / \partial \sigma_{ij}$, i.e. $\partial m_{ij} / \partial \sigma_{kl} = \partial^2 Q / \partial \sigma_{ij} \partial \sigma_{kl}$) normal to the potential function, derived at the final stress point. The traditional tangent stiffness tensor has a constant derivative, m_{ij} that is evaluated at the intersection point.

The derivation of the consistent tangent stiffness tensor can be traced back to the works of Runesson and Samuelsson[?] and Simo and Taylor.[?] As a consequence of consistency, the use of the consistent tangent stiffness tensor significantly improves the convergence characteristics of the overall equilibrium iterations, if a Newton scheme is used for the latter. Use of the consistent tangent stiffness tensor yields a quadratic convergence rate of the Newton equilibrium iterations. In what follows, we derive the consistent tangent stiffness tensor for single–vector return algorithms. A straightforward derivation of the two–vector return consistent tangent stiffness tensor is treated in detail by Jeremić and Sture,[?] as described earlier.

We start from the Backward Euler stress equation:

$$^{n+1}\sigma_{ij} = {}^{pred}\sigma_{ij} - \lambda \, E_{ijkl} \, {}^{n+1}m_{kl} \tag{32}$$

Differentiation of equation (32) and solving for $d\sigma_{mn}$ yields:

$$d\sigma_{mn} = R_{mnkl} \left(d\epsilon_{kl} - d\lambda \, {}^{n+1}H_{kl} \right) \tag{33}$$

where we have used definitions for $^{n+1}T_{ijmn}$ and $^{n+1}H_{kl}$ from equation (19) and have defined the *reduced stiffness tensor* as:

$$R_{mnkl} = \left({}^{n+1}T_{ijmn} \right)^{-1} E_{ijkl} \tag{34}$$

It turns out that the form of equation (33) is similar to the old *non consistent* form except for the change in E_{mnkl} to $R_{mnkl} = \left({}^{n+1}T_{ijmn} \right)^{-1} E_{ijkl}$ and the fact that the normal

to the potential surface is evaluated at the final stress position, and includes the change on flow direction due to hardening or softening, i.e. it is presented in form of ${}^{n+1}H_{kl} = {}^{n+1}m_{kl} + \lambda \left(\partial m_{kl}/\partial q_*\right)|_{n+1} h_*$.

We are assuming that the full consistency condition should hold at the final stress position ${}^{n+1}F = 0$ so that the consistency condition is:

$$d^{n+1}F = {}^{n+1}n_{ij}d\sigma_{ij} + {}^{n+1}\xi_* dq_* = 0 \tag{35}$$

The solution for the stress increment is available from equation (33), and the solution for $d\lambda$ is readily found:

$$d\lambda = \frac{{}^{n+1}n_{ij}R_{ijkl}d\epsilon_{kl}}{{}^{n+1}n_{ij}R_{ijkl} \; {}^{n+1}H_{kl} + {}^{n+1}\xi_* \; h_*} \tag{36}$$

By substituting equation (36) in equation (33) and solving for $d\sigma_{pq}$, we obtain:

$$d\sigma_{pq} = R_{pqkl}\left(d\epsilon_{kl} - \frac{{}^{n+1}n_{rs}R_{rsmn}d\epsilon_{mn}}{{}^{n+1}n_{ot}R_{otpq} \; {}^{n+1}H_{pq} + {}^{n+1}\xi_* \; h_*} \; {}^{n+1}H_{kl}\right) =$$

$$R_{pqkl}d\epsilon_{kl} - R_{pqkl}\frac{{}^{n+1}n_{rs}R_{rsmn} \; {}^{n+1}H_{kl}}{{}^{n+1}n_{ot}R_{otpq} \; {}^{n+1}H_{pq} + {}^{n+1}\xi_* \; h_*}d\epsilon_{mn} =$$

$$\left(R_{pqmn} - \frac{R_{pqkl}{}^{n+1}H_{kl}{}^{n+1}n_{ij}R_{ijmn}}{{}^{n+1}n_{ot}R_{otpq} \; {}^{n+1}H_{pq} + {}^{n+1}\xi_* \; h_*}\right)d\epsilon_{mn} =$$

$$ {}^{cons}E^{ep}_{pqmn}d\epsilon_{mn} \tag{37}$$

where the *Elastic Plastic Consistent Tangent Stiffness Tensor* is given by:

$${}^{cons}E^{ep}_{pqmn} = R_{pqmn} - \frac{R_{pqkl}{}^{n+1}H_{kl}{}^{n+1}n_{ij}R_{ijmn}}{{}^{n+1}n_{ot}R_{otpq} \; {}^{n+1}H_{pq} + {}^{n+1}\xi_* \; h_*} \tag{38}$$

It is worthwhile noting that the traditional, continuum tangent stiffness tensor E^{ep}_{pqmn} is recovered in the limit as $\lambda \to 0$:

$$\lim_{\lambda \to 0} {}^{cons}E^{ep}_{pqmn} = E^{ep}_{pqmn} = E_{pqmn} - \frac{E_{pqkl}m_{kl}n_{ij}E_{ijmn}}{n_{ot}E_{otpq}m_{pq} + \xi_* h_*} \tag{39}$$

since:

$$\lim_{\lambda \to 0} T_{ijmn} = \lim_{\lambda \to 0}\left(\delta_{im}\delta_{nj} + \lambda \; E_{ijkl} \; \frac{\partial m_{kl}}{\partial \sigma_{mn}}\bigg|_{n+1}\right) = \delta_{im}\delta_{nj}$$

$$\lim_{\lambda \to 0} R_{mnkl} = \lim_{\lambda \to 0}\left(T_{ijmn}\right)^{-1} E_{ijkl} = \left(\delta_{im}\delta_{nj}\right)^{-1} E_{ijkl} = E_{mnkl}$$

Jeremić & Sture

$$\lim_{\lambda \to 0} H_{kl} = \lim_{\lambda \to 0} \left({}^{n+1}m_{kl} + \lambda \frac{\partial m_{kl}}{\partial q_*}\bigg|_{n+1} h_* \right) = m_{kl}$$

An interesting observation is that the consistent tangent remains non symmetric, i.e. major symmetry is not restored, ${}^{cons}E^{ep}_{pqmn} \neq {}^{cons}E^{ep}_{mnpq}$, even in the case of associated flow rule, for which $m_{kl} = n_{kl}$, since:

$$(H_{kl})|_{m_{kl}=n_{kl}} = \left({}^{n+1}n_{kl} + \lambda \frac{\partial n_{kl}}{\partial q_*}\bigg|_{n+1} h_* \right)$$

and since, generally, $\lambda \partial n_{kl}/\partial q_* \neq 0$ the major symmetry is lost. It should be mentioned that for radial return flow rules[5] the symmetry is recovered. Major symmetry is also recovered in the limit as $\lambda \to 0$.

4   Implementation and Results

We have presented the Backward Euler algorithm and now we briefly present the material model used in the error assessments, namely the isotropic hardening or softening elasto–plastic MRS–Lade model.[?] We, then introduce a novel error measure, that proved more intuitive in assessing the overall algorithm accuracy. Then we illustrate one incremental step on the constitutive level and provide error estimates in terms of iso–error maps for various stress regions. Finally, we give a brief assessment of overall, finite element convergence rates obtained by using the consistent tangent stiffness tensor.

4.1   MRS-Lade Elasto–Plastic Model

The MRS-Lade elastic-plastic model for granular materials[?] is a further development of Lade's three-invariant model for cohesionless soils.[?] The model has been used to simulate the behavior under both high and low effective stresses levels. In order to better simulate the complex behavior of these materials, the MRS-Lade model features:

- a two–surface formulation, comprising of a smooth cone surface and a smooth cap surface intersecting in plane curve (ellipse segment) in the deviatoric plane,[?]

---

[5]Associated for example with von Mises criterion and isotropic hardening only.
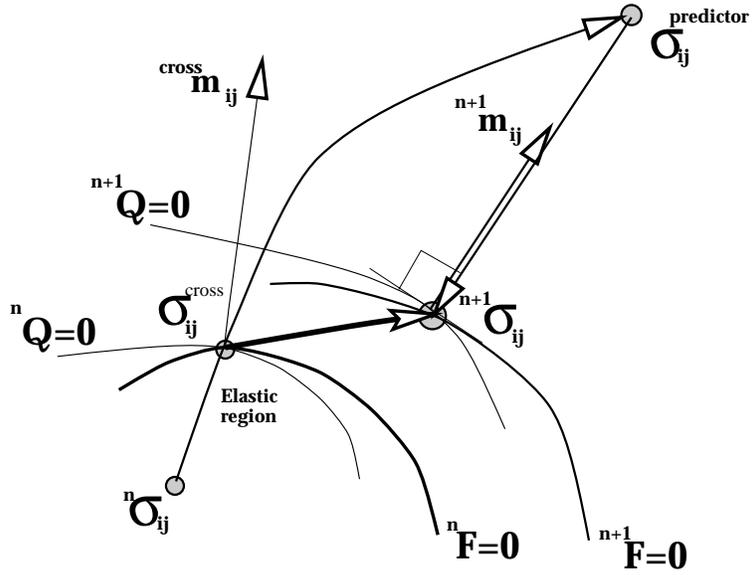
Figure 1: Pictorial representation of integration algorithms in computational elasto–plasticity: Backward schemes.
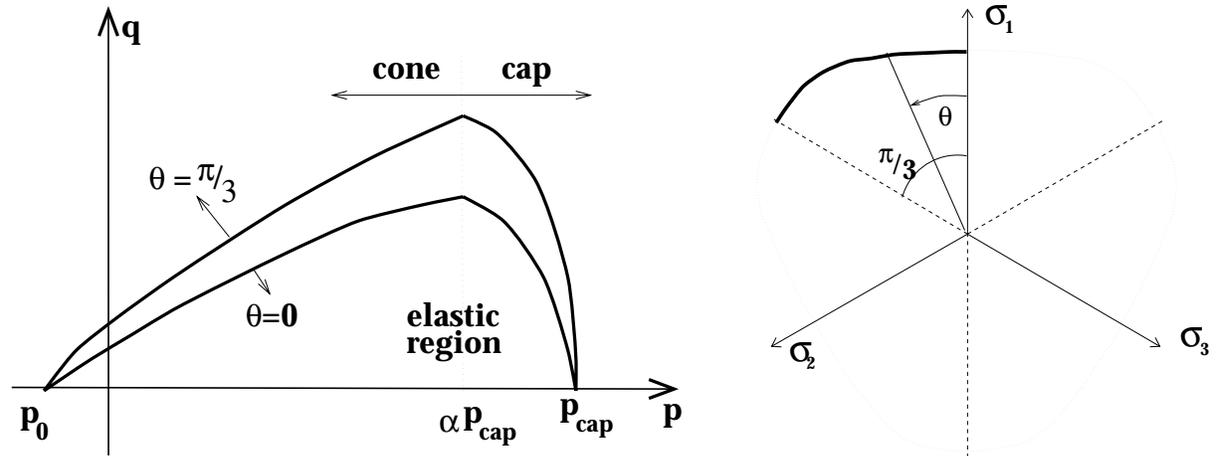

Figure 2: Trace of the MRS-Lade model in $p - q$ and deviatoric space. The definition of $p - q$ can be found in appendix.

- Hardening and softening variables for both surfaces are based on dissipated plastic work,

- a non-associated flow rule in the meridian plane and an associated flow rule in the deviatoric plane of the cone region, and a associated flow rule in the cap region,

- ability to model cohesive strength and a curved meridian in the cone region.

Here, we only briefly illustrate the shape of MRS–Lade yield surface $F = 0$ in Figures 2 and 3. Detailed discussion is presented by Sture, Runesson Macari-Pasqualino.[?] The shape of potential surface Q is very similar to the yield surface, i.e. traces in deviatoric plane are the same, and the difference accounting for dilatancy effects is reflected in a different trace in the meridian plane.

4.2 Error Measurement

The error measure for the Backward Euler algorithm was chosen to be the relative error in the energy norm between a single load step to the final stress point position, and an "exact" final position. The term "exact" is somewhat misleading, since the exact or closed form solution for the general elasto–plastic problem remains to be found. The "exact" return point is simply the point obtained by subincrementing the given strain increment in a certain number of subincrements, say 50, using the same integration scheme, in this case the Backward Euler method.

Different methods were used to asses the accuracy of integration algorithms in computational plasticity. Early works[?,?,?,?] related to the von Mises criterion were simply using the difference between the single step return angle θ and the "exact" angle. This is advantageous in the case of the von Mises yield surface, since the only error developed in integrating the elasto–plastic differential equations in the deviatoric plane, is in the value of the angle θ. Later works[?,?] have measured errors in terms of vector norms of differences between a single step solution and the "exact" solution. The need to devise a new error measure stems from the many types of yield criteria that are dependent on all three stress invariants (defined in Appendix A), i.e. p, q and θ, or, alternatively I_1, J_{2D} and J_{3D}.

In this work we will use the normalized distance between "exact" and single step solution defined in the D_{klpq} metric[6]. This distance is determined by taking the energy norm of the difference of the stress tensors between the two stress points. The energy norm is defined as:

$$\|\sigma_{ij}\|^2 = \sigma_{ij} D_{ijkl} \sigma_{kl} \tag{40}$$

It was assumed that the *unit* length, measured in the energy norm, is from the origin to the stress state represented by $p = 1.0 \ kN/m^2$, $q = 0.0 \ kN/m^2$ and $\theta = 0$. All errors, i.e. differences between the single step solution and the "exact" solution are compared to that unit length. The *normalized distance*[7] is then defined as:

$$\delta_{normalized} = \frac{\|^{n+1}\sigma_{ij}^{50steps} - {}^{n+1}\sigma_{ij}^{singlestep}\|}{\|p^{unit}\|} \tag{41}$$

This error measure is more intuitive, since it actually represents the normalized distance between two stress points.

4.3   Algorithm illustration

Figure (4) depicts the convergence of the Backward Euler integration scheme in stress space. Table (1) summarizes three stress paths, i.e. the points in the p, q and θ space for the three elastic–predictor plastic corrector returns. The Forward Euler return is actually the tangent path from the intersection point. The point is somewhat further away than the other two return points, since the Forward Euler scheme uses the return direction at the intersection point, thus yielding a more inclined return direction. The semi Backward Euler return uses the normal at the trial or elastic predictor point, so the return direction is somewhat less inclined than, for example the Backward Euler direction, and a return point is closer to the starting point compared to the other two methods. Neither method satisfies the yield condition at the final stress point. The Backward Euler

---

[6]D_{klpq} is the elastic compliance fourth order tensor, defined in terms of *Lamé* coefficients λ and μ as:

$$D_{klpq} = \frac{-\lambda}{2\mu \left(3\lambda + 2\mu\right)} \, \delta_{kl}\delta_{pq} + \frac{1}{4\mu} \left(\delta_{kp}\delta_{lq} + \delta_{kq}\delta_{lp}\right)$$

[7]according to the definition $p = -1/3 \ \sigma_{kk}$, the normalized distance is the same as the unit distance along any of three principal stress axis.
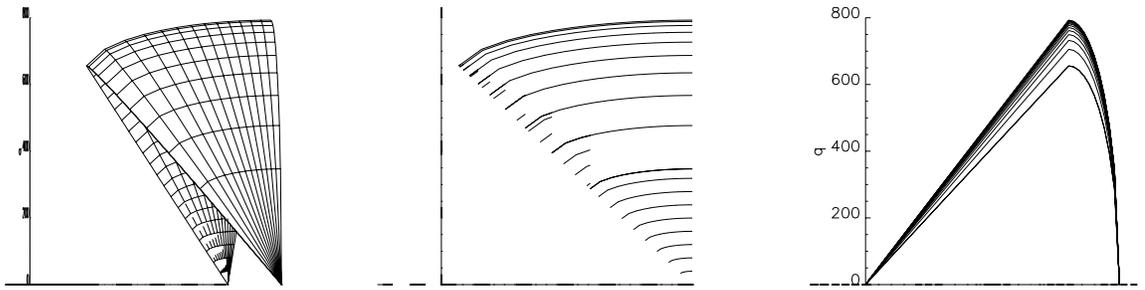
Figure 3: MRS-Lade cone/cap yield surface. Only the first sextant (where $\sigma_1 \geq \sigma_2 \geq \sigma_3$) is shown.
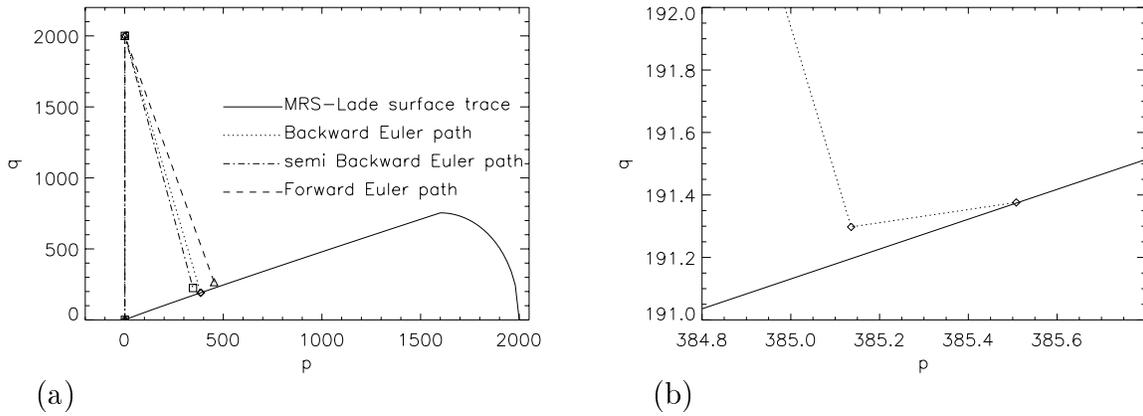

(a)

(b)

Figure 4: (a) Actual paths of the Backward Euler, semi Backward Euler and Forward Euler schemes, and the last two iterations. (b) Magnified picture in the region of the solution. In the triaxial meridian plane. Units: kN/m^2.

return is performed at two levels, where the first level comprises the predictor phase by using either a Forward Euler step or semi Backward step. The second, iterative level brings the stress point to the yield surface. In the present example, only two iterations are needed after the predictor step to obtain the solution. Figure (4)(b) depicts two stress points, the first located a small distance away from the surface and the second and final point, very close to the surface.

4.4   Error Assessment

The accuracy analysis of the derived algorithm is assessed in a number of examples. We describe stress regions, where the accuracy of the algorithm was assessed in Figure (5) :

- Region 1 is close to the zero stress state, and is defined on the cone portion of the MRS-Lade yield surface in the meridian $p - q$ plane . The region extends into the tension stress state, and the apex gray region.

- Region 2 is in the deviatoric plane of the MRS-Lade cone part defined by $p = 1.0 \ kN/m^2$, while $\theta \in [0.0 - \pi/3]$.

- Region 3 is in the meridian plane $\theta = \pi/3$, and covers the cap yield surface.

- Region 4 is in the meridian plane $\theta = \pi/3$, close to the corner gray area. Both cone and cap surfaces are covered as well as the corner gray region.

- Region 5 is defined in the meridian plane, $\theta = \pi/3$, on the cone portion of the MRS-Lade yield surface, in vicinity of the confining pressure of $p = 500.0 \ kN/m^2$.

Region 1. The starting point for the accuracy assessment of Region 1 is at $p = 1.0 \ kN/m^2$. The lower inclined line in Figure (6)(region 1.), represents the trace of the cone yield surface in the meridian plane, and the dashed line represents the border between the cone region and the apex gray region. This iso–error map gives a good picture of the general trend, i.e. the further away from the surface the stress point is, the errors become more pronounced. Some areas of nonuniformity are found, especially just above the trace line and about the vertical axis. After closer investigation of nonuniformities close to the trace line it appears that the errors represent rather small values and the predictor points that are closer to the surface needed fewer iterations to satisfy the consistency

position points	$p\ kN/m^2$	$q\ kN/m^2$	F_{cone}	Error
starting	1.0	0.42389	-0.177	-
elastic predictor	1.0	2000.0	2669.185	-
forward Euler	453.491	266.321	54.403	84.368
semi Backward Euler	346.232	224.672	66.142	45.115
Backward Euler step 1	385.136	191.298	0.126	-
Backward Euler step 2	385.508	191.376	$8.141\ 10^{-7}$	12.075
"exact" return	397.013	196.876	$7.696\ 10^{-7}$	-

Table 1: Stress paths for the Backward Euler, semi Backward Euler and Forward Euler schemes. In meridian plane $\theta = \pi/3$. Errors are normalized to unit length.
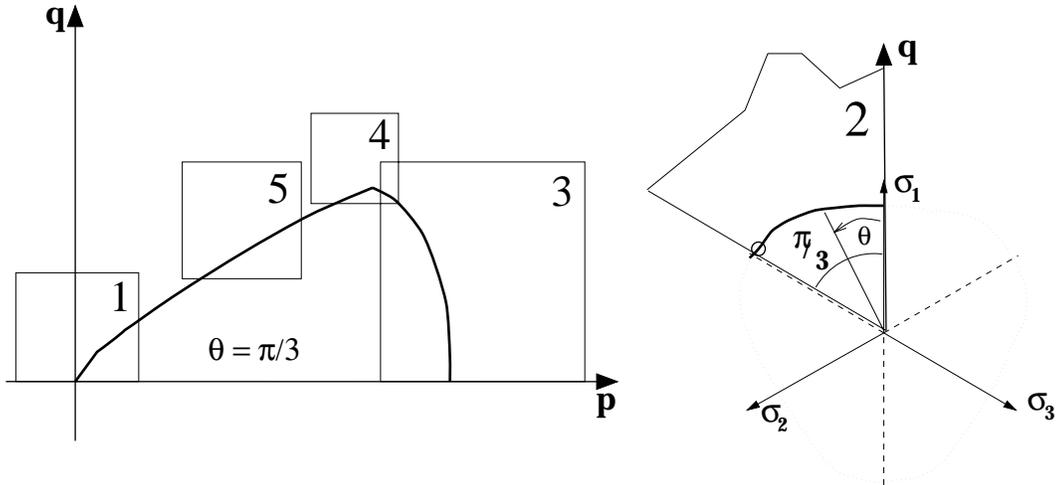

Figure 5: Accuracy assessment regions in p, q and θ invariant space.

Jeremić & Sture

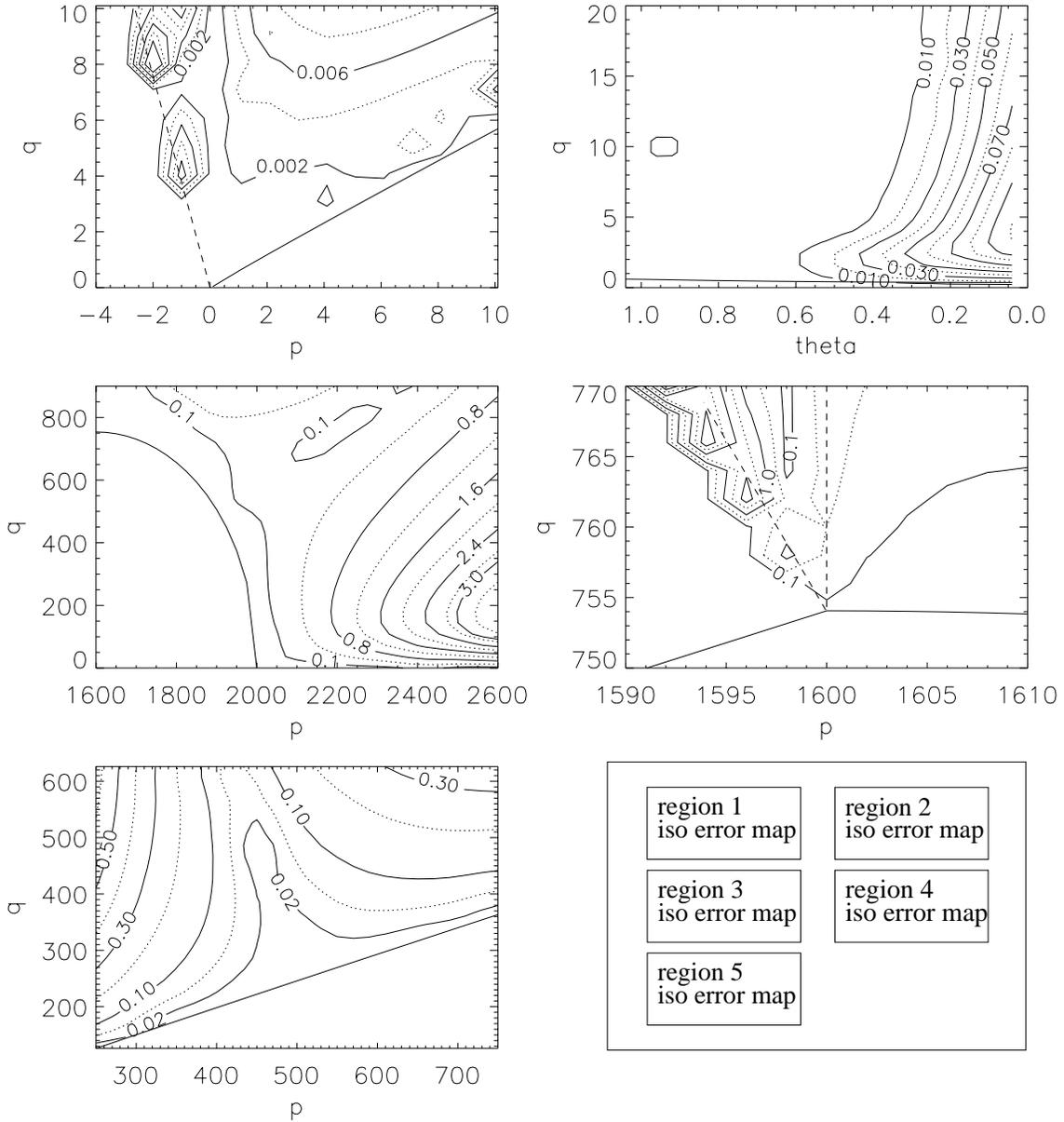Figure 6: Iso–error maps for the different regions of MRS–Lade yield criterion. Errors normalized to unit length. Figure units kN/m^2.
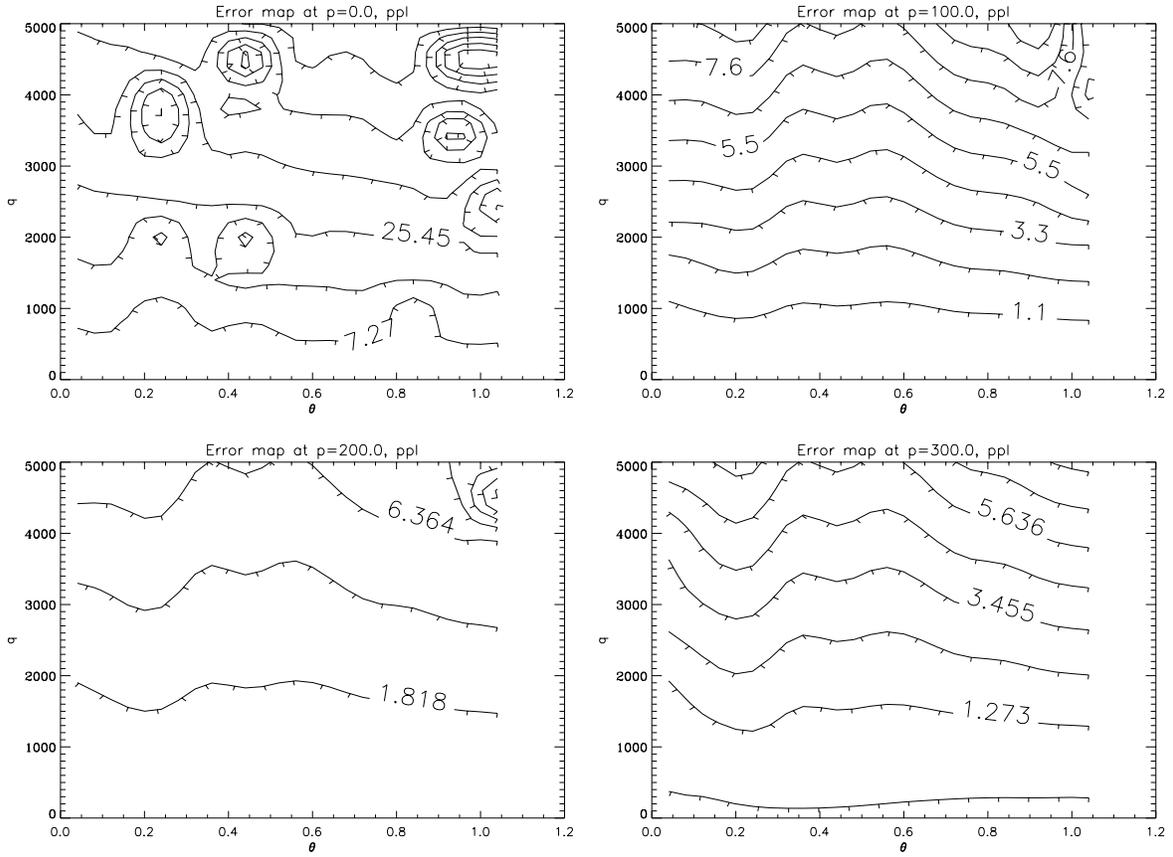
Jeremić & Sture

Figure 7: Large excursions ($\epsilon^{dev} \approx 3\%$) in deviatoric plane (region 2.). Slices of iso–error surface at $p = 0.0; 100.0; 200.0; 300.0 kN/m^2$. Errors normalized to unit length. Figure units kN/m^2.

Jeremić & Sture

condition, i.e. to decrease the value of the yield function below a predefined tolerance, while those that have predictor points further away needed more iterations, thus resulting in final stress states that satisfied yield criteria with lower tolerance. However, for larger excursions away from the yield surface, the error pattern increase smoothly. Another region of nonuniform errors is located close to the border line. It appears that while the one–step solution returns to the cone surface close to the apex point, the "exact" solution is substepping toward the apex point, and since the "exact" solution tends to push the return point further away, it ends up at the apex point. For the stress predictor points located further away in the apex gray region the return is to the apex point in both cases.

Region 2. The starting point for accuracy assessment in Region 2 is located on the yield surface at $\theta = \pi/3 \approx 1.04$, while $p = 1.0 \ kN/m^2$ and $q = 0.6 \ kN/m^2$, or at the left end of the yield surface trace on Figure (6)(region 2.). It is evident that the errors increase as the angular distance from the starting point increases. The error increase is fast for large tangential steps, yet after a certain magnitude of q the algorithm is quite insensitive to the values of q, while changes in θ create most of the error. Yet another non-uniform region is discovered near the value $q = 10.0 \ kN/m^2$. This is attributed to the highly curved yield surface in the vicinity of $\theta = \pi/3$.

Figures 7 depicts the behavior of the algorithm for large strain steps ($\approx 3\%$) in the deviatoric direction while the stress is varied from $p = 0.0 \ kN/m^2$ to $p = 300.0 \ kN/m^2$. The non–uniform areas on the first iso–error map, at $p = 0.0 \ kN/m^2$ are actually better solution since the algorithm failed to converge for specific strain increments and the subincrementation cure was initiated. The low confinement domain, around $p = 0.0 \ kN/m^2$ is highly nonlinear, which places a great demand on a constitutive driver. Once the low confinement domain is cleared, errors are increasing in a relatively smooth manner. Unlike the iso–error map on Figure 6(region 2.), which depicted errors for very small strain increments, all the errors, for large deviatoric excursions are controlled by the deviatoric component of strain.

Region 3. The iso–error map for Region 3 depicts the cap portion of the surface, and it illustrates the behavior of the algorithm for a starting point located in the elastic region at $p = 1600.0 \ kN/m^2$ and $q = 0.0 \ kN/m^2$. The trace of the cap surface is visible as the curved line on the left in Figure 6(region 3.). It is interesting to note that the more curved

region, toward the intersection with the cone yield surface, shows smaller errors than the more leveled region located toward the p axis. This observation follows the conclusion made by de-Borst and Feenstra[?] with regard to the Backward Euler algorithm applied to Hill's criterion.

Region 4. The corner domain is especially trouble prone. Difficulties encountered are basically topological in nature. All the predictor stress states that fall in the corner gray region are supposed to end up on the line in the deviatoric plane that connects the two surfaces. The main problem with the present definition of the flow direction is that for some stress paths, a single step starting from one region, a cone for example, returns to the same region, while the "exact" solution will jump and return to the other region. Figure (6)(region 4.) depicts the corner region iso–error map. Errors are accumulated near the left boundary line of the corner region. The reason is that for the predictor stresses near the border line but located in the cone region, the return is to the cone surface, close to the corner point. The "exact" solution tends to push the return point further away, thus returning to the cap region.

Region 5. The iso–error maps for Region 5, on Figure (6), represent the behavior of the algorithm on the cone area of the yield surface. The pattern is similar to that already observed. The more tangential the stress path is, the larger is the error. The predictor stress path that follows the flow direction m_{ij} suffers from the inexact integration of hardening or softening rule only, while the stress subspace integration is exact.

4.5   Global Picture: FEM Convergence

The convergence properties of consistent tangent stiffness tensor upon implementation in a finite element program ⊞[8] are briefly depicted on one incremental step of a simple drained triaxial numerical experiment on a loose sand from Figure 8.

In Figure (4.5) we follow one increment through three different types of control:[?] mixed, or full arc-length control (FU), λ–control (F) and displacement control (U). Since this was a displacement driven numerical experiment, λ–control actually mimics a dominant, vertical displacement control. Table (4.5) also shows that the use of the *consistent*

---

[8]Finite Element Interpreter, our testbed program, under development using **nDarray** and ⊞Mtools class libraries written in C++ programming language.
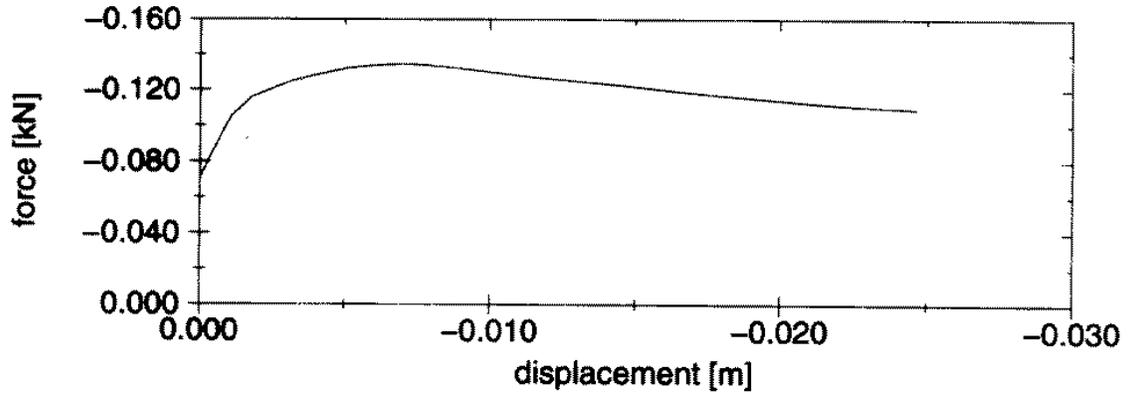
Figure 8: Non–linear response for the dry triaxial sand specimen.

$\downarrow$iter.,$\|\mathbf{r}\| \rightarrow$	FU	F	U
prev.(1)	$0.00e+0$	$0.00e+0$	$0.00e+0$
pred.(2)	$8.05e-4$	$2.11e-3$	$1.03e-3$
(3)	$1.91e-4$	$7.70e-4$	$2.29e-4$
(4)	$3.83e-5$	$2.79e-4$	$3.93e-5$
(5)	$6.76e-6$	$9.95e-5$	$5.55e-6$
(6)	–	$3.39e-5$	–
(7)	–	$9.90e-6$	–

Table 2: Convergence results for one increment and different types of control.
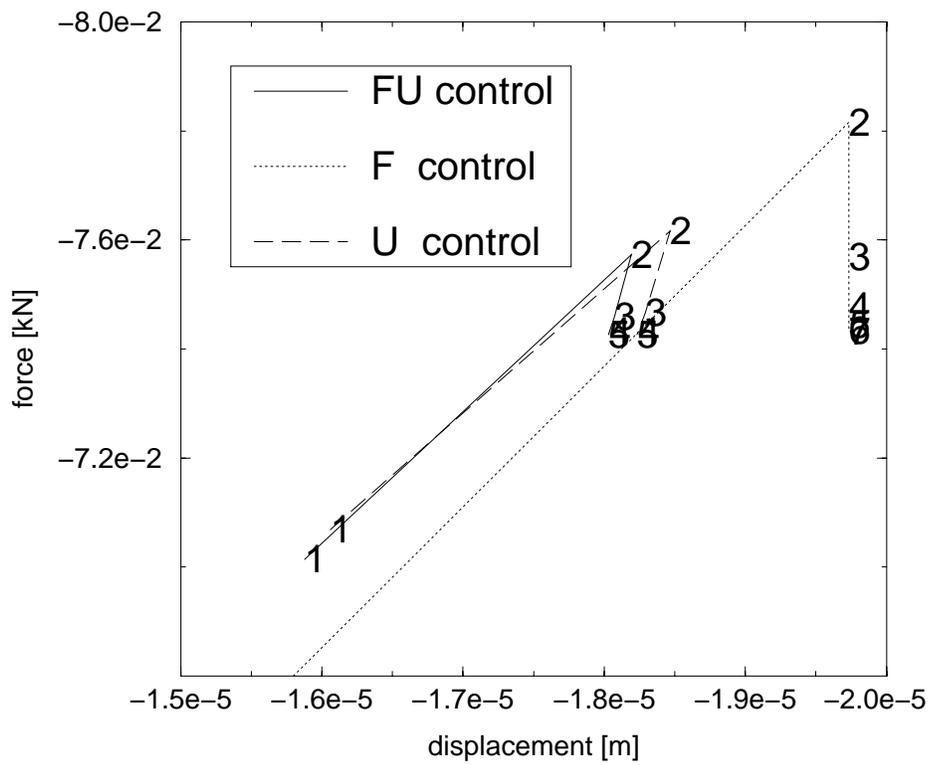
Jeremić & Sture

Figure 9: Iterative paths for one increment and different types of control.

tangent stiffness tensor in building the system stiffness matrix together with a full New-ton iterative solution scheme at the global level results in a fast convergence rate for the residual norm $\|\mathbf{r}\|$. At the end, converged points are close[9] to the actual equilibrium path. As for all path dependent problems, actual difference in the step length introduces additional error.

5   Concluding Remarks

In this paper we have presented a fully implicit, Backward Euler algorithm for integrating directly, in the expanded stress – internal variable space, elasto–plastic constitutive equations for isotropic elasto–plastic hardening or softening geomaterial models. Derivation of the algorithm and the resulting consistent stiffness tensor were kept as general as possible, thus making the implementation of other isotropic hardening or softening elasto–plastic material models an relatively easy task.

The algorithm was applied to the pressure sensitive, three stress invariant, hardening or softening MRS–Lade elasto–plastic material model. The algorithm performance was assessed on a number of examples, and fast convergence at the global, finite element level was shown, if one uses the consistent tangent stiffness tensor in building finite element matrices. A set of useful stress invariants derivatives was provided in both closed and finite difference form.

Acknowledgment

---

[9]Close here means within convergence tolerance.

6   Appendix

A   Gradients to the Potential Function

In the derivation of the *Backward Euler algorithm* and the *Consistent Tangent Stiffness Tensor* it is necessary to derive the first and the second derivatives of the potential function. The function Q is the function of the stress tensor σ_{ij} and the plastic variable tensor q_*. In this section we present derivatives with respect to the stress tensor σ_{ij}. It is assumed that any stress state can be represented with the three stress invariants p, q and θ given in the following form:

$$p = -\frac{1}{3}I_1 \quad ; \quad q = \sqrt{3J_{2D}} \quad ; \quad \cos 3\theta = \frac{3\sqrt{3}}{2}\frac{J_{3D}}{\sqrt{(J_{2D})^3}} \tag{42}$$

$$I_1 = \sigma_{kk} \quad ; \quad J_{2D} = \frac{1}{2}s_{ij}s_{ij} \quad ; \quad J_{3D} = \frac{1}{3}s_{ij}s_{jk}s_{ki} \quad ; \quad s_{ij} = \sigma_{ij} - \frac{1}{3}\sigma_{kk}\delta_{ij} \tag{43}$$

Stresses are here chosen as positive in tension. The definition of Lode's angle θ in equation (42) implies that $\theta = 0$ defines the meridian of conventional triaxial extension (CTE), while $\theta = \pi/3$ denotes the meridian of conventional triaxial compression (CTC).

A.1   Analytical Gradients

The first derivative of the function Q in stress space is:

$$\frac{\partial Q\,(p,q,\theta)}{\partial\sigma_{ij}} = \frac{\partial Q}{\partial p}\frac{\partial p}{\partial\sigma_{ij}} + \frac{\partial Q}{\partial q}\frac{\partial q}{\partial\sigma_{ij}} + \frac{\partial Q}{\partial\theta}\frac{\partial\theta}{\partial\sigma_{ij}} \tag{44}$$

and subsequently the first derivatives of the chosen stress invariants are

$$\frac{\partial p}{\partial\sigma_{ij}} = -\frac{1}{3}\,\delta_{ij} \quad ; \quad \frac{\partial q}{\partial\sigma_{ij}} = \frac{3}{2}\frac{1}{q}s_{ij} \tag{45}$$

$$\frac{\partial\theta}{\partial\sigma_{ij}} = \frac{3}{2}\frac{\cos 3\theta}{q^2\sin 3\theta}s_{ij} - \frac{9}{2}\frac{1}{q^3\sin 3\theta}t_{ij} \quad \text{where:} \quad t_{ij} = \frac{\partial J_{3D}}{\partial\sigma_{ij}} \tag{46}$$

The second derivative of the function Q in stress space is

$$\frac{\partial^2 Q\,(p,q,\theta)}{\partial\sigma_{pq}\partial\sigma_{mn}} =$$

$$\left(\frac{\partial^2 Q}{\partial p^2}\frac{\partial p}{\partial\sigma_{mn}} + \frac{\partial^2 Q}{\partial p\partial q}\frac{\partial q}{\partial\sigma_{mn}} + \frac{\partial^2 Q}{\partial p\partial\theta}\frac{\partial\theta}{\partial\sigma_{mn}}\right)\frac{\partial p}{\partial\sigma_{pq}} + \frac{\partial Q}{\partial p}\frac{\partial^2 p}{\partial\sigma_{pq}\partial\sigma_{mn}} \quad +$$

$$+ \left(\frac{\partial^2 Q}{\partial q\partial p}\frac{\partial p}{\partial\sigma_{mn}} + \frac{\partial^2 Q}{\partial q^2}\frac{\partial q}{\partial\sigma_{mn}} + \frac{\partial^2 Q}{\partial q\partial\theta}\frac{\partial\theta}{\partial\sigma_{mn}}\right)\frac{\partial q}{\partial\sigma_{pq}} + \frac{\partial Q}{\partial q}\frac{\partial^2 q}{\partial\sigma_{pq}\partial\sigma_{mn}} \quad +$$

$$+ \left(\frac{\partial^2 Q}{\partial\theta\partial p}\frac{\partial p}{\partial\sigma_{mn}} + \frac{\partial^2 Q}{\partial\theta\partial q}\frac{\partial q}{\partial\sigma_{mn}} + \frac{\partial^2 Q}{\partial\theta^2}\frac{\partial\theta}{\partial\sigma_{mn}}\right)\frac{\partial\theta}{\partial\sigma_{pq}} + \frac{\partial Q}{\partial\theta}\frac{\partial^2\theta}{\partial\sigma_{pq}\partial\sigma_{mn}} \tag{47}$$

and the second derivatives of the stress invariants are

$$\frac{\partial^2 p}{\partial\sigma_{pq}\partial\sigma_{mn}} = \emptyset \quad ; \quad \frac{\partial^2 q}{\partial\sigma_{pq}\partial\sigma_{mn}} = \frac{3}{2}\frac{1}{q}\left(\delta_{pm}\delta_{nq} - \frac{1}{3}\delta_{pq}\delta_{nm}\right) - \frac{9}{4}\frac{1}{q^3}\,s_{mn}s_{pq} \tag{48}$$

$$\frac{\partial^2\theta}{\partial\sigma_{pq}\partial\sigma_{mn}} =$$

$$-\left(\frac{9}{2}\frac{\cos 3\theta}{q^4\sin 3\theta} + \frac{27}{4}\frac{\cos 3\theta}{q^4\sin^3 3\theta}\right)s_{pq}\,s_{mn} + \frac{81}{4}\frac{1}{q^5\sin^3 3\theta}\,s_{pq}\,t_{mn} +$$

$$+\left(\frac{81}{4}\frac{1}{q^5\sin 3\theta} + \frac{81}{4}\frac{\cos^2 3\theta}{q^5\sin^3 3\theta}\right)t_{pq}\,s_{mn} - \frac{243}{4}\frac{\cos 3\theta}{q^6\sin^3 3\theta}\,t_{pq}\,t_{mn} +$$

$$+\frac{3}{2}\frac{\cos 3\theta}{q^2\sin 3\theta}\,p_{pqmn} - \frac{9}{2}\frac{1}{q^3\sin 3\theta}\,w_{pqmn} \tag{49}$$

where:

$$w_{pqmn} = \frac{\partial t_{pq}}{\partial\sigma_{mn}} = s_{np}\delta_{qm} + s_{qm}\delta_{np} - \frac{2}{3}s_{qp}\delta_{nm} - \frac{2}{3}\delta_{pq}s_{mn}$$

$$p_{pqmn} = \frac{\partial s_{pq}}{\partial\sigma_{mn}} = \delta_{mp}\delta_{nq} - \frac{1}{3}\delta_{pq}\delta_{mn}$$

Alternatively, if one decides to work with I_1, J_{2D} and J_{3D} stress invariants, the useful set of derivatives is:

$$\frac{\partial I_1}{\partial\sigma_{ij}} = \delta_{ij} \quad ; \quad \frac{\partial J_{2D}}{\partial\sigma_{ij}} = s_{ij} \quad ; \quad \frac{\partial J_{3D}}{\partial\sigma_{pq}} = s_{qk}s_{kp} - \frac{2}{3}\delta_{pq}J_{2D} = t_{pq} \tag{50}$$

Jeremić & Sture

$$\frac{\partial^2 J_{2D}}{\partial \sigma_{pq} \partial \sigma_{mn}} = \frac{\partial s_{pq}}{\partial \sigma_{mn}} = \delta_{mp}\delta_{nq} - \frac{1}{3}\delta_{pq}\delta_{mn} = p_{pqmn} \tag{51}$$

$$\frac{\partial^2 J_{3D}}{\partial \sigma_{pq} \partial \sigma_{mn}} = \frac{\partial t_{pq}}{\partial \sigma_{mn}} = s_{np}\delta_{qm} + s_{qm}\delta_{np} - \frac{2}{3}s_{qp}\delta_{nm} - \frac{2}{3}\delta_{pq}s_{mn} = w_{pqmn} \tag{52}$$

A.2 Finite Difference Gradients

After having developed the closed form, analytical derivatives the authors asked themselves: "is there a simpler way of finding these derivatives and how can we check our derivations?". Dennis and Schnabel[?] propose the *finite difference method* for approximating derivatives if these derivatives are not analytically available and as a tool to check your analytical derivatives if they are derived. Another good reason for developing alternative gradients is that for $\theta = 0, \pi/3$ gradients are not defined, i.e. indefinite terms as $1/0$ are appearing. One possible solution is the use of *l'Hospital's rule*. The solution to that problem in this work went in a different direction, i.e. instead of aiming for the analytical form, numerical derivatives are derived.

We should recall that for a function f of a single variable, the finite difference approximation to $f'(x)$, by using *forward finite difference approach*, is given by:

$$a = \frac{f(x+h) - f(x)}{h} \tag{53}$$

where h is a vanishingly small quantity. The first derivative of F (or Q) with respect to the stress tensor σ_{ij} elements is[10]:

$$^{approx}F_{,ij} = \frac{F(\sigma_{ij} + h_{ij} + h_{ji}) - F(\sigma_{ij})}{X \, h_{ij}} \tag{54}$$

where X is an integer number that takes values of 1 or 2 depending on whether the element being computed is on the diagonal[11] or off, respectively, and h_{ij} is the step size which,

---

[10]no sum convention implied throughout this section, just the position of the element.

[11]since the stress tensor σ_{ij} is symmetric, change in one non-diagonal element triggers the other to be changed as well.

Jeremić & Sture

because of *finite precision arithmetic*, is a variable, a small number, h, that is multiplied with the current stress value so that the relative order of magnitude is retained.

The accuracy of the finite difference approximation to the analytical derivatives is closely bound to the step size h_{ij}. It was suggested[?] that for functions given by the simple formula, the number h should be close to $h = \sqrt{macheps}$, while for more complicated functions that number should be larger. Here *macheps* is the so called *machine epsilon.* It is defined as the smallest distinguishable positive number[12], such that $1.0 + macheps > 1.0$ yields true on the given computer platform.

For example, double precision arithmetics (64 bits), on the `Intel 80x86` platform yields `macheps= 1.08E-19` while on the `SUN SPARCstation` and `DEC` platforms `macheps= 2.22E-16`.

It has been found that in the case of yield or potential functions the best approximation of analytical gradients is obtained by using $h = \sqrt{macheps}\ 10^3$. The three order of magnitude increase in the finite difference step is due to a rather complicated formula for yield and potential functions. The error in the approximation, $^{approx.}F_{,ij}$ is found to be after the Nth decimal place, where N is the order of h.

Second derivative approximations for one variable function are given in the form:

$$a = \frac{(f(x + h_i e_i + h_j e_j) - f(x + h_i e_i)) - (f(x + h_j e_j) - f(x))}{h_i h_j} \tag{55}$$

If the first derivatives are available in closed form, one could use equations (54) just by replacing the function values with tensor values for analytical derivatives. However, if the analytic derivatives are not available, one has to devise a formula that will create a fourth order tensor from the changes in two stress tensors, σ_{ij} and σ_{kl}. Using the scheme employed in equation (55) the following formula has been devised:

$$^{approx}Q_{,ijkl} = \frac{(Q(\sigma_{mn} + h_{ij} + h_{kl}) - Q(\sigma_{mn} + h_{ij})) - (Q(\sigma_{mn} + h_{kl}) - Q(\sigma_{mn}))}{Y\ h_{ij} h_{kl}}$$

$$\tag{56}$$

and Y is an integer number that takes values of 1, 2 or 4 depending on whether the element computed is on the major diagonal, minor diagonal or off, respectively.

---

[12]in a given precision, i.e. float (32 bits), double (64 bits) or long double (80 bits).

It should be pointed out that numerical derivatives are much slower to compute than closed form derivatives. However, flexibility gained by employing two different schemes for obtaining such important tensors is very important.

Jeremić & Sture